ORIGINAL ARTICLE

Analysis of three-roller continuous and synchronous calibration process of straightness and ovality for large thin-walled pipes considering the weld

Xueying Huang[1] · Jun Zhao[3] · Gaochao Yu[3] · Rongzhi Li[2,3] · Bangbang Ma[2,3] · Chunge Wang[2]

Abstract

Large thin-walled pipes are commonly used in the field of oil and gas pipeline transmission. In general, the straightness and ovality of pipes cannot meet the industry standard. They are required to be calibrated. However, the weld affects the straightness and ovality of pipes, which in turn has significant influence on the quality and safety of pipelines. Based on previous research, the three-roller continuous and synchronous calibration process of straightness and ovality for large thin-walled pipes is feasible. To explore the influence of the weld on this process, a comparative study of welded pipes and seamless pipes is done using finite element (FE) method. The FE model of this process is established according to the experimental results of the micro-tensile experiment and the Vickers hardness test of the actual welded pipe. The FE results show that there is a slight distortion at the inlet end of the welded pipe, and its length is 20 mm. Maximum deviation value is 0.55 mm. Distortion regions and deviation values are small and are found to be negligible. The difference between welded pipes and seamless pipes based on the residual straightness and residual ovality is very small. The residual straightness does not exceed 2‰, and the residual ovality is not more than 1%. The changed trend of each roller over time of the welded pipe is almost consistent with the seamless pipe. Especially, the experimental results and FE results demonstrate good agreement.

✉ Chunge Wang
  wangchunge@nit.zju.edu.cn

  Xueying Huang
  huangxueying@nbufe.edu.cn

  Jun Zhao
  zhaojun@ysu.edu.cn

  Gaochao Yu
  gch_yu@ysu.edu.cn

  Rongzhi Li
  202021010262@stumail.ysu.edu.cn

  Bangbang Ma
  bond@stumail.ysu.edu.cn

1 School of Digital Technology and Engineering, Ningbo University of Finance and Economics, Ningbo City 315175, People's Republic of China

2 School of Mechanical and Energy Engineering, NingboTech University, Ningbo City 315100, People's Republic of China

3 Key Laboratory of Advanced Forging & Stamping Technology and Science (Yanshan University), Ministry of Education of China, Qinhuangdao City 066004, People's Republic of China

1 Introduction

Oil and gas have long become the world's important energy with development potential. Large thin-walled pipes have a wide range of application prospects in paving oil and gas pipelines in cold areas or deep seas. According to the American Petroleum Institute's industry standard ANSI/API Spec. 5L, the ovality and straightness of formed pipes have been required strictly in real production. The ovality does not exceed ± 0.75% of pipe nominal outer diameter. The straightness is not greater than 0.2% of the total length of pipe [1]. During the process of producing large thin-walled pipes, the ovality and straightness cannot meet the industry standards due to the factors such as welding thermal stress, material properties, and technical equipment [2–4]. Therefore, formed pipes need to be calibrated.

The existing calibration processes of ovality and straightness are done separately. At present, the calibration process of ovality mainly includes the whole-diameter calibration process [5, 6], the over-bending calibration process [7–9],
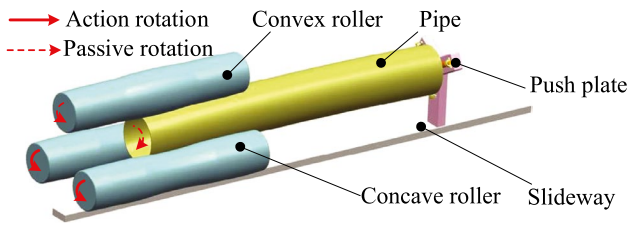
Fig. 1 Schematic diagram of the calibration process

and the roll-type calibration process [10, 11]. Generally, straightness calibration techniques include the pressure straightening [12, 13] and the cross-roll straightening [14–16]. Because the deformation process between ovality calibration and straightness calibration restricts each other, the flattening problem of large thin-walled pipes cannot be solved [17]. It is difficult to adjust both the ovality and straightness to optimal levels, which also seriously affects on-site welding and pipeline safety [18]. Zhao et al. proposed the three-roller continuous and synchronous calibration process of straightness and ovality firstly [19]. This process unified the ovality calibration process and the straightness calibration process creatively, enabling cooperative calibration of large thin-walled pipes. In view of this process, Yu et al. [18] put forward a roller-shape design method. The feasibility of this process was verified by FEM for the first time. Subsequently, Huang et al. [20] established a bidirectional mechanical model in the axial and circumferential directions based on the pipe deformation mechanism. This model further proved that the pipe's deformation involves the reciprocating bending processes of circumferential and axial directions. Additionally, the influence of process parameters on pipe calibration results was analyzed. The calibration strategy was also presented through experiments.

The above study of pipe calibration process did not consider the influence of the weld on the calibration results. However, it can possibly influence the ovality, straightness, and final shape of the pipe. This was critical as it has been found
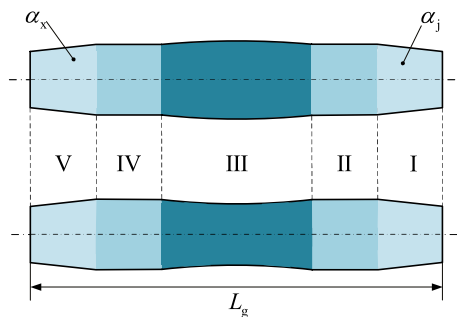

Fig. 3 Curvature distribution of Section III — n-segment curvature

that the collapse pressure of the pipe is highly dependent on the final shape of the pipe [21–24]. In addition, corrosion was the main failure cause of submarine pipeline [25]. Corrosion has a great negative influence on the pipe service life, and high welding residual stress will accelerate corrosion and reduce the strength of the pipe [26]. During the process of using super-large natural gas pipelines, due to pressurization, it was easy to cause local deformation. There was a negative impact on service safety of piping materials [27]. Taking X80 pipeline steel containing weld area as the research object, Wu et al. [28] adopted different tensile pre-deformation to simulate the unidirectional tensile stress formed by pipeline pressurization. The influence of work hardening caused by co-strain between weld and parent on the tensile properties of pipeline steel was also studied. Weld line is an important indicator to determine whether oil and gas transmission pipelines can operate safely [29]. Consequently, it is of great significance to study the welds' influence on large thin-walled pipes in the calibration process, which provides technical support for the normal operation of oil and gas transmission pipelines.

Build on previous research, the three-roller continuous and synchronous calibration process of straightness and ovality of large thin-walled pipes was feasible [18, 30]. In order to explore the influence of the weld on this process, a comparative

Fig. 2 Schematic diagram of roller-shape. Section I: loading section; Section II: ovality calibration section; Section III : ovality and straightness calibration section; Section IV : ovality complement calibration section; Section V : unloading section
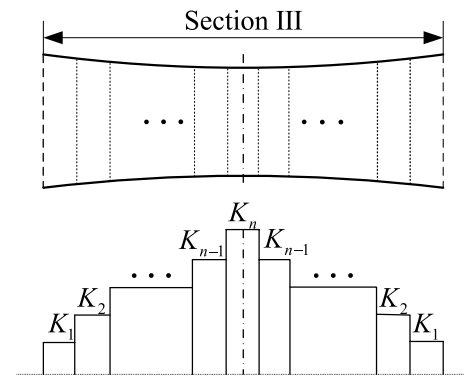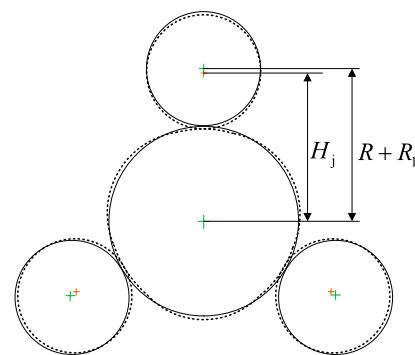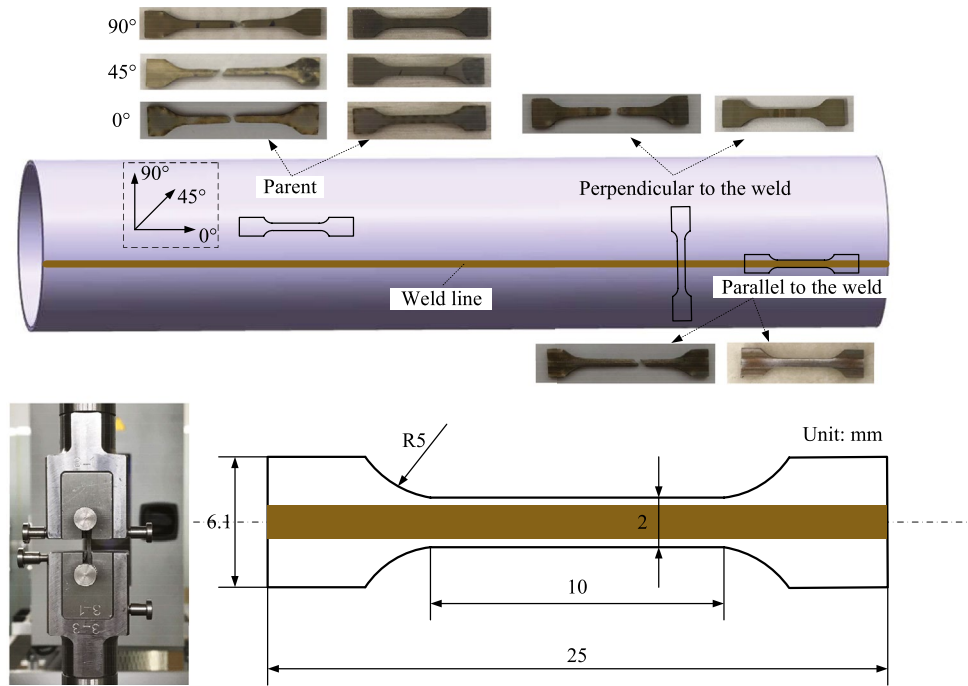

Fig. 4 Diagram of loading parameters

Fig. 5 Cutting position and size of samples

study between welded pipes and seamless pipes is carried out using the FE method. First of all, based on the micro-tensile test, it is believed that the 304 pipes' materials for the parent and weld zone are isotropic, respectively. The mechanical property parameters are further obtained. Secondly, the size of the weld zone is determined through Vickers hardness test, with analyzing its microstructure performance. As a result, the finite element model (FEM) is established assuming that the material follows the isotropic-kinematic hardening model. The experimental results verify the correctness of FE results.

2 Three-roller continuous and synchronous calibration process

The three-roller continuous and synchronous calibration process of straightness and ovality for large thin-walled pipes is shown in Fig. 1. The process' main working parts

are three parallel rollers, including a convex roller (upper roller) and two concave rollers (lower rollers).

Calibration process Before experiment, each roller pushes the same radial reduction toward the pipe's central axis. During the experiment, two concave rollers rotate simultaneously driven by servo motors. This makes the pipe and convex roller rotate under the action of friction. At the same time, the servo motor drives the push plate to make the pipe move along the slideway, thus finishing the calibration process.

The schematic diagram of roller-shape is shown in Fig. 2. As shown in Fig. 2, both ends of the roller are loading section (Section I) and unloading section (Section V), both of which are truncated cone shape. Section II and IV are ovality calibration sections, which are cylindrical in shape. Section

Fig. 6 Stress–strain response of parent and weld zone along different directions
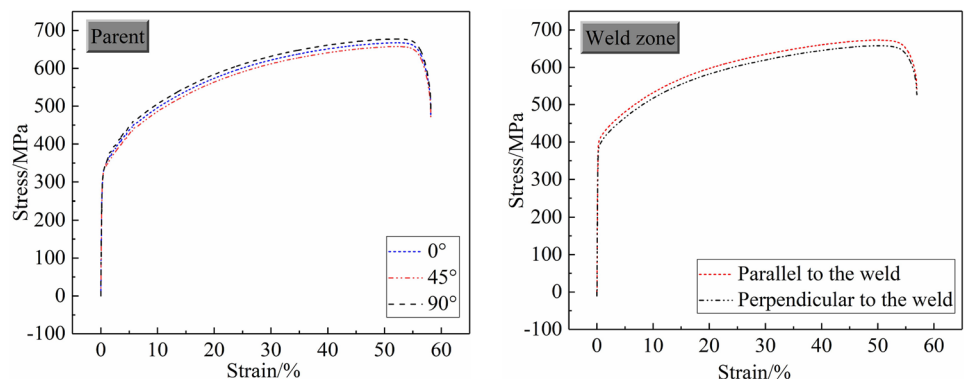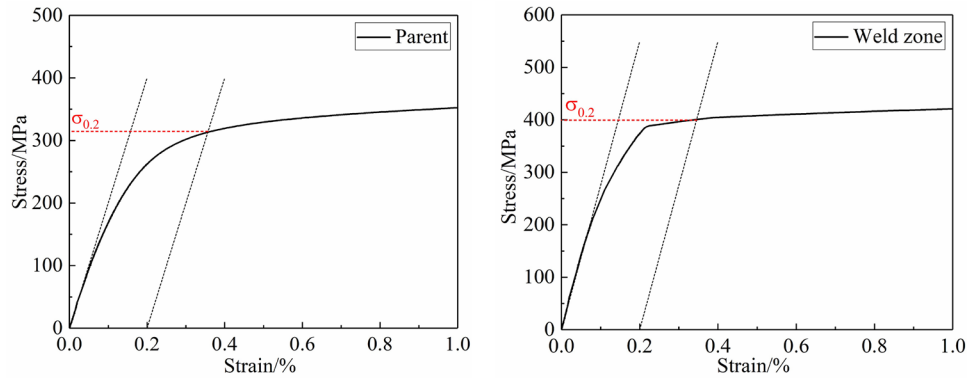
Fig. 7 Solution of the yield strength of the parent and the weld zone

III is ovality and straightness calibration section. The upper roller part is convex and the lower roller part is concave [20].

The curvature distribution of Section III is shown in Fig. 3. Section III is composed of *n* tangent arcs with changing curvature, whose curvature is gradually reduced from the middle to both ends. That is, K_1 to K_n gradually increases in value, and K_n is the maximum curvature of Section III.

Figure 4 is a schematic diagram of the loading parameter. Three rollers load the same radial reduction toward the pipe center, and the stroke of each roller is recorded as *H*.

$$H = R_1 + R - H_j \tag{1}$$

where *H* is the radial reduction, R_1 is the roller radius, *R* is the pipe radius, and H_j is the distance from the pipe's center to the center of roller after loading.

3 Model building

To reproduce the material's behavior characteristics and make the actual simulation analysis reflect the actual situation more accurately, the following work has been carried out.

3.1 Material performance parameters

The material used in this paper is 304 stainless steel welded pipe, and the welding wire is also the same material. First, uniaxial micro tension tests are performed on parent material's tensile specimens with a rolling direction of 0°, 45°, and 90° according to the API 5L standard [1]. In addition,

depending on the position of weld, tensile specimens containing weld zones are selected for uniaxial micro tensile tests. Among them, it includes two directions, such as perpendicular to the weld and parallel to the weld. The cutting position and size of tensile specimens are shown in Fig. 5.

According to the micro-tensile tests, the stress–strain curves of the parent and the weld zone along different directions are obtained, as shown in Fig. 6. The stress–strain curves with different directions obtained by the parent and the weld zone are basically coincident. Therefore, it can be considered that the materials of the parent and the weld zone show isotropy.

The solution of yield strength of the parent and the weld zone, as shown in Fig. 7. In this paper, the stress value at a strain value of 0.2% is the yield limit, that is, the yield strength value of the material. The mechanical properties of the material of the parent and weld zone are given in Table 1. The chemical composition of the material is given in Table 2.

Table 1 Mechanical properties of the parent and weld zone

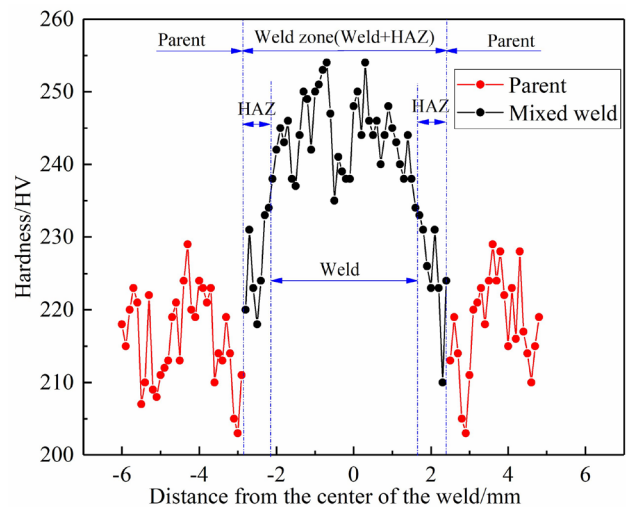| Materials	Young's modulus E/GPa	Yield strength σ_s/MPa	Plastic tangent modulus D/MPa	Poisson's ratio ν
Parent	210	314	2720	0.3
Weld zone	265	398	2642	0.3

Fig. 8 Microhardness distribution of mixed weld specimen containing weld zone and parent

Table 2 Chemical composition of 304 stainless steel (wt. %)

C	Si	Mn	S	P	Cr	Ni	Fe
≤0.08	≤1.00	≤2.00	≤0.30	≤0.045	18.00~20.00	8.00~11.00	–

3.2 Geometric parameters

The size of the weld zone can be determined by the microhardness distribution [31]. Microhardness specimen cutting is performed on mixed weld specimen containing weld zone and parent. Then, the specimen is submitted to a Vickers hardness test in FM-ARS9000 microhardness tester. The microhardness distribution of the weld zone and parent of the 304 stainless steel welded pipe is illustrated in Fig. 8. As can be observed in Fig. 8, the microhardness at the weld is the greatest, reaching 240–250 HV. The microhardness of the parent is minimal, about 210–220 HV. The farther away from the center of the weld, the smaller the microhardness.

Based on the microhardness distribution of the weld, heat affected zone (HAZ) and parent, the width of the weld is founded to be about 3.6 mm, and the width of each HAZ is about 0.78 mm. Since the width of HAZ is smaller than that of the weld, and the microhardness of HAZ is close to the parent's microhardness, the influence of HAZ on the pipe forming process is ignored.

The microstructure pictures of the area near the weld, as shown in Fig. 9. Figure 9(a) shows the microstructure of the parent and its matrix is austenite. Figure 9(b) is the microstructure of the HAZ near the parent. From Fig. 9(a) and (b), the grain size of the parent is 48.7 μm and the grain size of the HAZ is 117 μm. The significant increase in grain size is due to the action of welding heating on both sides of the weld. Figure 9(c) shows the microstructure of the weld. The directionality of the weld microstructure is relatively strong, and the whole is dendritic crystals.

3.2.1 FEM

The FEM of the pipe calibration process is established using the software ABAQUS, as shown in Fig. 10. In this paper, 304 stainless steel pipes with an outer diameter of 140 mm and a thickness of 2 mm are used as research objects. Considering the influence of welds on the calibration process, a FE analysis of seamless pipes and welded pipes is performed. The mechanical properties of the pipe are given in Table 1. The geometric dimensions of the pipe and the roller are shown in Tables 3 and 4, respectively.

With a kinematic hardening model, the pipe is set as a deformable body. The pipe-wall is divided into 4 layers along the thickness, and the pipe is discretized by 8-node linear hexagonal nonconforming mode elements. Select the continuum distributing coupling method to couple the center point of the pipe circle-section and the pipe cross-section boundary, and select all 6 degrees of freedom for the constrained area. The three rollers are set as discrete rigid

Fig. 9 Microstructure pictures of the area near the weld: **a** parent; **b** HAZ adjacent to parent; **c** weld
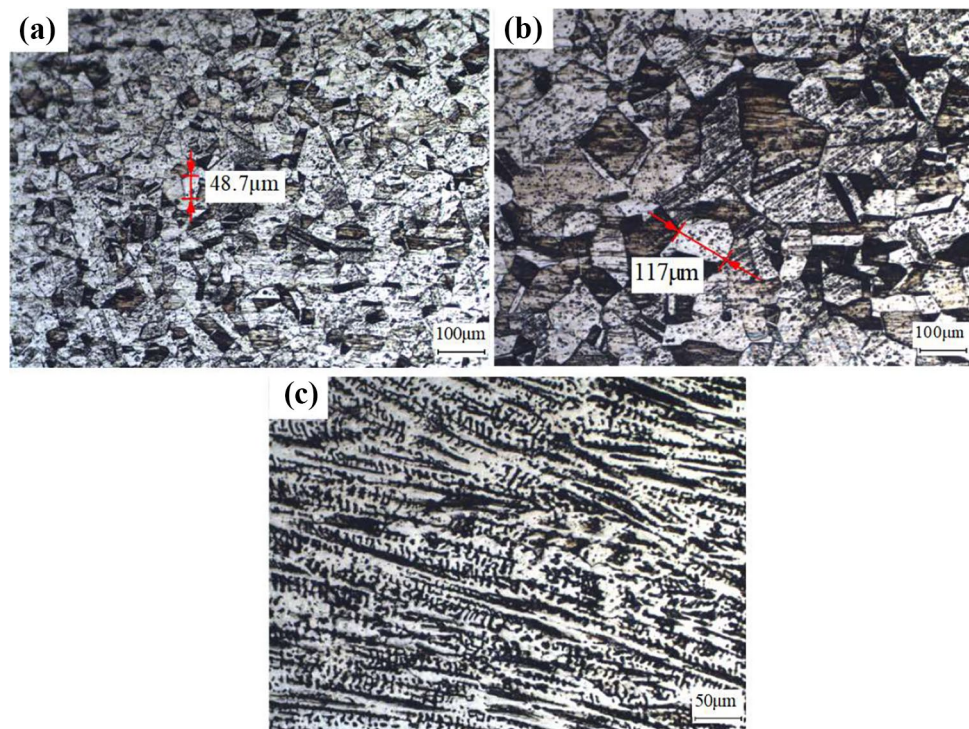
Fig. 10 Finite element model:
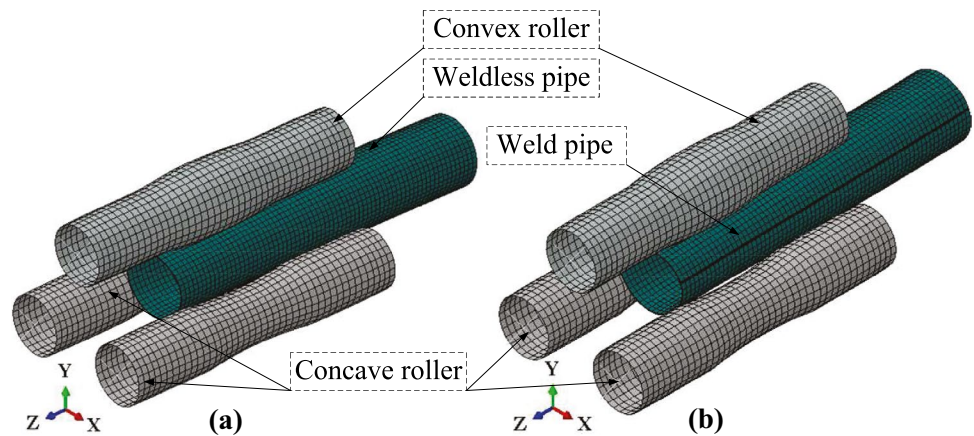**a** seamless pipe; **b** welded pipe

Table 3 Geometric dimensions of the pipes

Material	Outside diameter D_p/mm	Length L_p/mm	Thickness t/mm	Initial ovality	Initial straightness
304	140	700	2	5%	10‰

bodies. The contact between the pipe and each roller is set to pure master–slave contact and motion contact conditions, and the coefficient of friction is 0.2.

4 Results and discussion

4.1 Calibration process

The equivalent stress distribution of a 304 welded pipe during the calibration process is shown in Fig. 11. During the process of advancing the pipe, the equivalent stress of the pipe inner and outer layers gradually increases. The equivalent stress of the pipe's parent exceeds its yield stress (314 MPa). The equivalent stress at the pipe weld exceeds its yield stress (398 MPa). Thus, the pipe enters the elastoplastic deformation state from the elastic deformation state. In the whole deformation process, the sections of circumferential and axial undergo multiple reciprocating bending. So that the curvature of the circumferential and axial directions is unified to the same value and direction, respectively. In the process of pushing out the pipe, the equivalent stress is gradually reduced with

elastic unloading occurs. The calibration process is completed after springback.

The equivalent stress distribution of a 304 welded pipe at the Section III is analyzed. It can be observed in Fig. 12 that there are three positive bending regions and three reverse bending regions along the circumferential direction. They are uniformly distributed. In addition, the stress distribution of the seamless pipe is the same as that of the welded pipe [32].

## 4.2 Comparative analysis of welded pipes and seamless pipes

4.2.1 Residual stress

Figure 13 and Fig. 14 are the residual stress distribution of seamless and welded pipes, respectively. It is well known that residual stress affects the service performance of pipes directly. As can be seen from Fig. 13, there is no instability or distortion in the cross-section of the pipe. Maximum residual stress is 186.5 MPa, which is less than the yield stress of the pipe (314 MPa). The larger residual stresses are mainly concentrated at the exit end of the pipe, namely the unloading section. The main reason for the above situation is the inconsistent deformation of inner and outer layers at the end of pipe. By analyzing the equivalent stress distribution after calibration, the contact state between the roller and the pipe can be inferred, which provides a certain reference for the design of roller-shape.

Table 4 Geometric dimension of the rollers

| Outside diameter D_g/mm	Length L_g/mm	Proportion of rollers	Taper of Section I α_j/rad	Taper of Section V α_x/rad	K_n/mm^{-1}	Roller shape curve of Section III
120	600	1:2:4:2:1	0.033	0.025	0.001	$0.16x^2 - 0.0004y^2 - 1 = 0$

Fig. 11 Equivalent stress distribution of a 304 welded pipe during the calibration process. **a** Loading section. **b** Ovality and straightness calibration section. **c** Unloading section
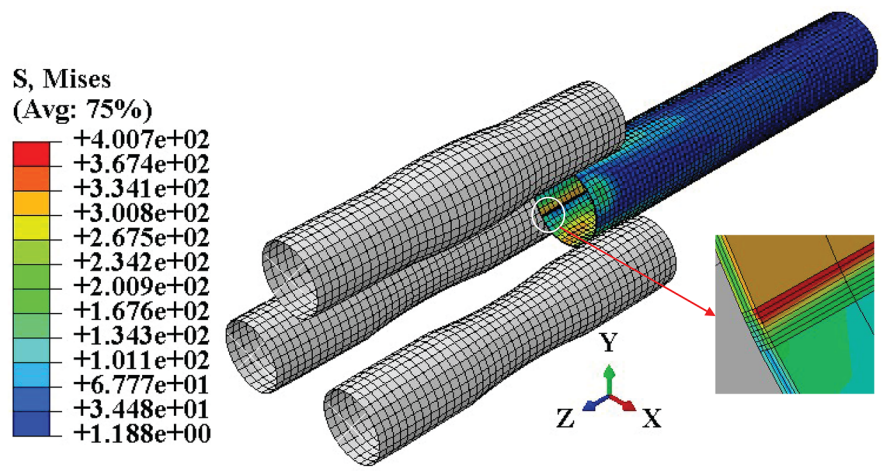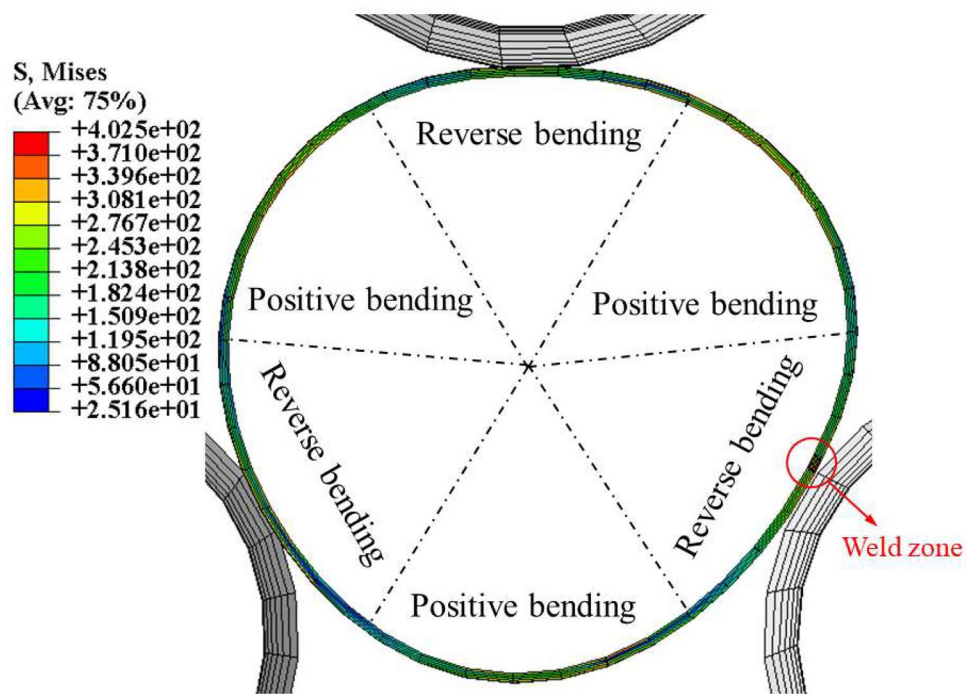

(a) Loading section
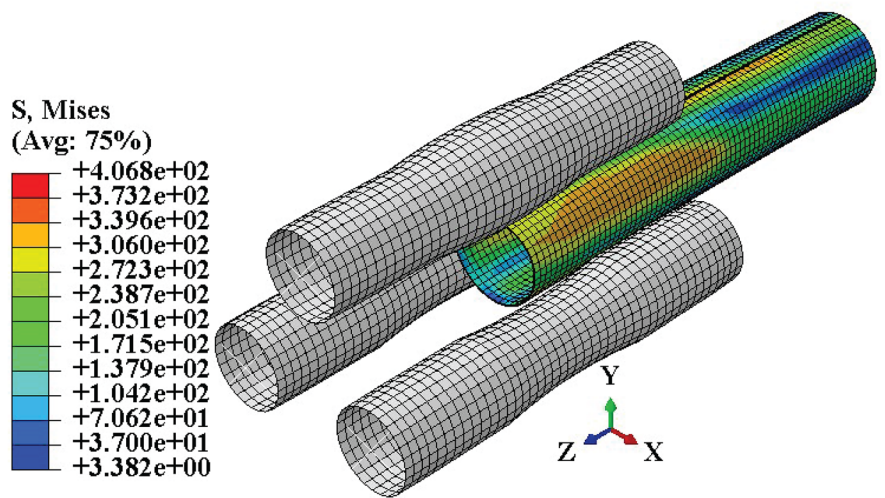
(b) Ovality and straightness calibration section
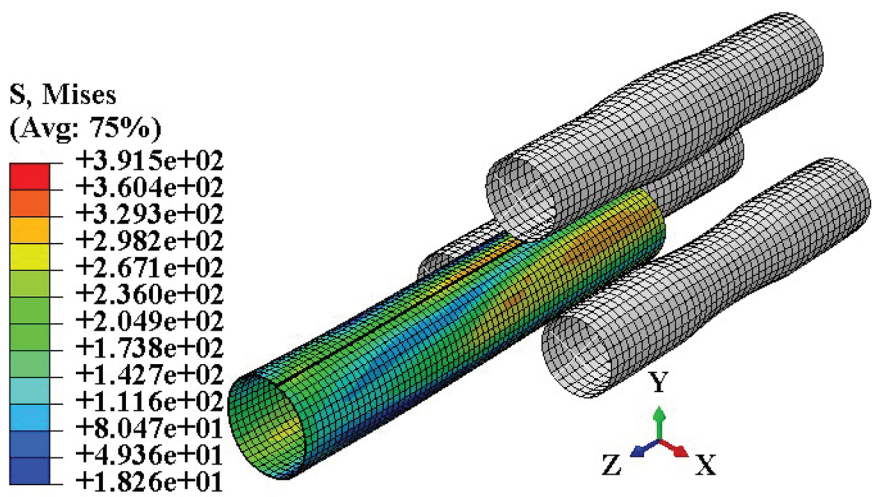
(c) Unloading section

Fig. 12 Equivalent stress distribution of a 304 welded pipe at the Section III

The distribution of residual stress in the welded pipe is shown in Fig. 14. The position coordinates of each point in the circumference direction of the weld from the inlet end are shown in Fig. 15. The datum plane is the circumferential cross section of the pipe. As can be seen from Figs. 14 and 15, the inlet end of the pipe is the contact area between the pipe and the loading section, and the residual stress is large with a maximum value of 370 MPa. In the area 0–20 mm from the inlet end, a slight cross-sectional distortion occurs at the weld, and the maximum deviation value is 0.55 mm. This is related to the downward control speed of the radial reduction H. Since the distortion area and the maximum deviation value are very small, they can be ignored. The residual stress values in other areas are small, and the range of stress value is 119.8 MPa to 161.3 MPa. Therefore, the process is still considerable for the calibration effect of the welded pipe.

4.3 Residual ovality

The geometry of the circular section of seamless pipes and welded pipes before and after the simulation is shown in Fig. 16. Figure 16 (a) shows the geometry of a seamless pipe before and after the simulation. The initial ovality of the pipe is 5%, and the residual ovality is 0.59%, which meets the industry standard [1]. Figure 16 (b) shows the geometry of a welded pipe before and after the simulation. Its residual ovality is 0.68%, which is not much different from the residual ovality of the seamless pipe. The result also meets the industry standard [1].

4.3.1 Residual straightness

The pipe busbar of a seamless pipe and a welded pipe before and after the simulation are shown in Figs. 17 and 18. Figure 17 shows the pipe busbar of a seamless pipe before and
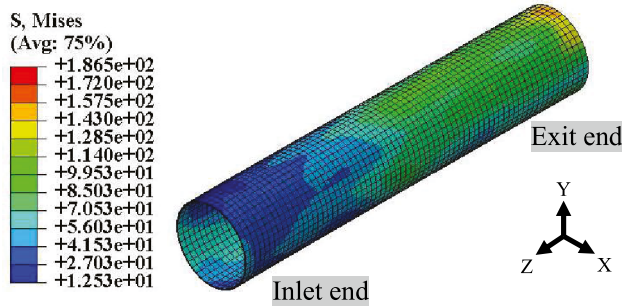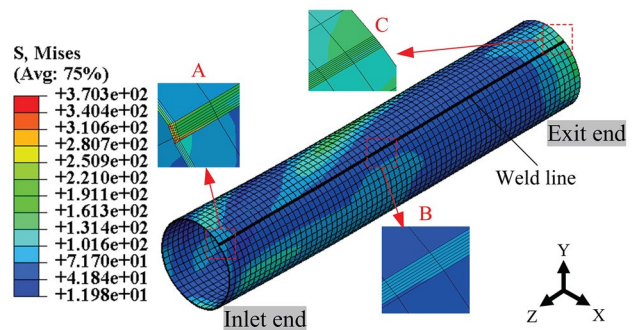

Fig. 13 Residual stress distribution of seamless pipes

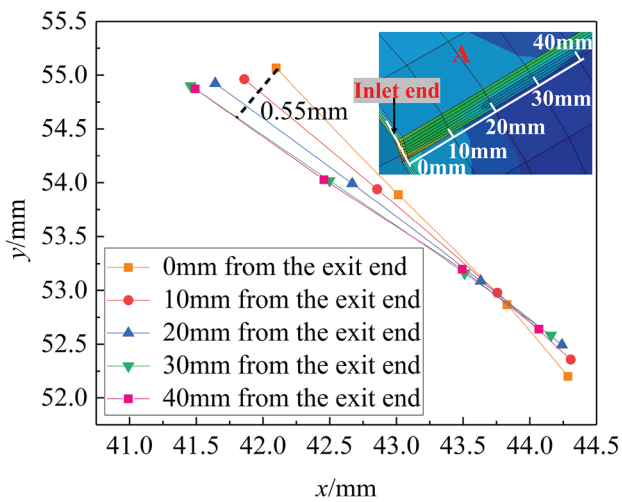**Fig. 14** Residual stress distribution of welded pipes

Fig. 15 Position coordinates of each point in the circumference direction of the weld from the inlet end

after the simulation. The initial straightness of the pipe is 10‰, and the residual straightness is 1.12‰, which meets the industry standard [1]. Figure 18 shows the pipe busbar of a welded pipe before and after the simulation. Its residual straightness is 1.6‰; the result also meets the industry standard [1].

4.3.2 Loading force of each roller

The change of each rollers' loading force with time is shown in Figs. 19 and 20. This process has a total of 2300 s. 0–230 s is the loading section (Section I), and the loading force of each roller increases with time gradually; 230–690 s is the ovality calibration section (Section II); 690–1610 s is the ovality and straightness calibration section (Section III); 1610–2070s is the ovality complement calibration section (Section IV); 2070–2300 s is the unloading section (Section V); the loading force of each roller gradually decreases with time.

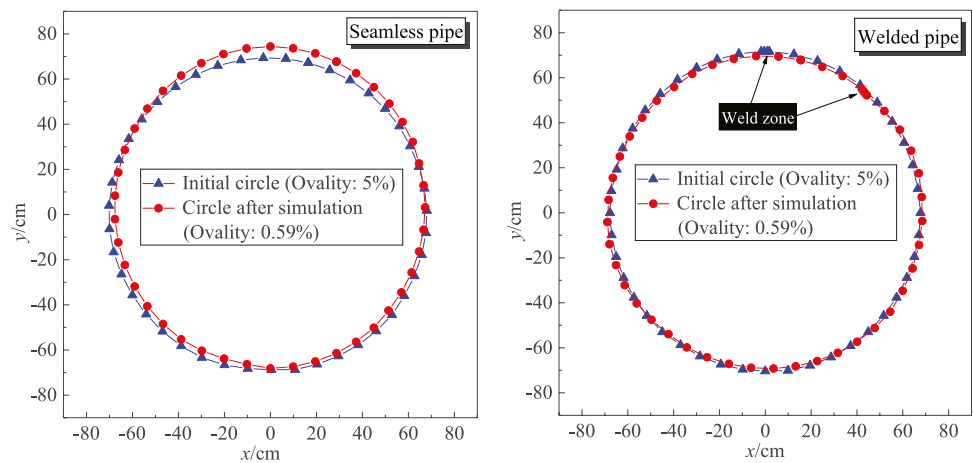**Fig. 16** Geometry of the circle section of seamless pipes and welded pipes before and after the simulation

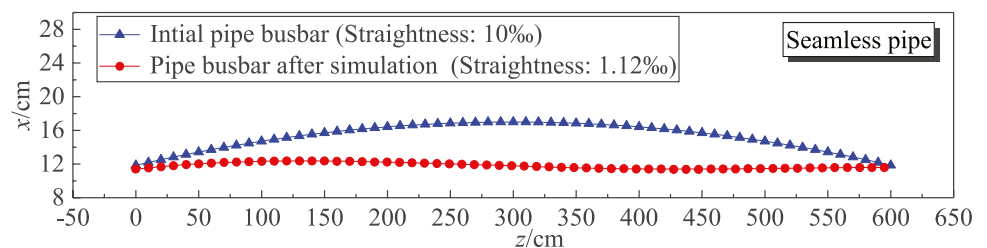**Fig. 17** Pipe busbar of a seamless pipe before and after the simulation

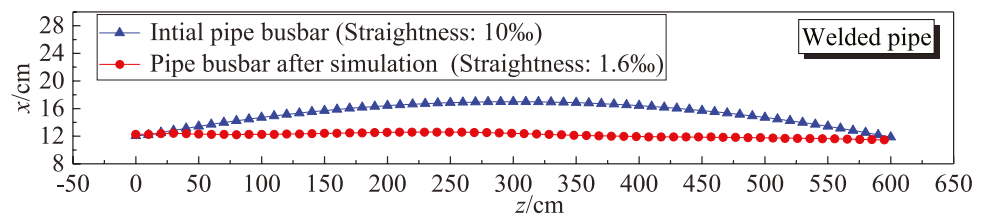**Fig. 18** Pipe busbar of a welded pipe before and after the simulation

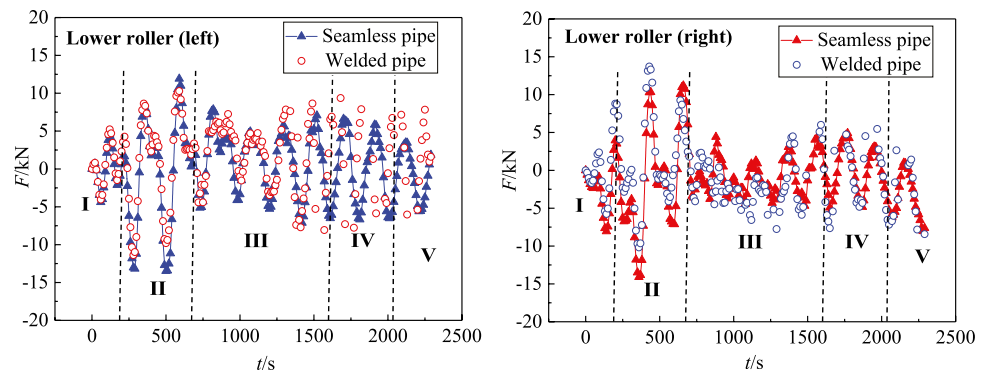**Fig. 19** Change of the lower rollers' loading force with time

Figure 19 shows the change in loading force of the two lower rollers with time. It can be seen from Fig. 19 that the change of loading force with time of a seamless pipe and a welded pipe is consistent approximately. Since the shape of two lower rollers is concave at the Section III, the loading force is smaller compared to adjacent sections. In addition, the loading force of the Section II is greater than that of the Section IV. The reason is that the pipe shape that has just entered the Section II is not standard and requires a greater loading force. The maximum loading force of the welded pipe and the seamless pipe does not exceed 15 kN.

Figure 20 shows the change in loading force of the upper roller with time. It can be seen from Fig. 20 that the change of loading force with time of a seamless pipe and a welded pipe is consistent approximately. Since the upper's shape is convex at the Section 3, the loading force reaches its maximum at this section. Throughout the calibration process, the loading force of the upper roller increases, stabilizes, and decreases with time. The maximum loading force of the welded pipe and the seamless pipe does not exceed 5 kN.
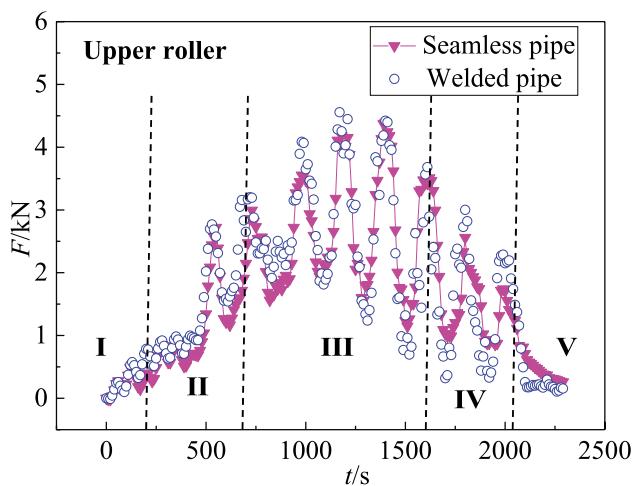
Therefore, the influence of the weld on rollers' loading force is small and can be ignored. The loading force of each roller whether seamless pipes or welded pipes is consistent with time.

5 Experimental validation

The experimental device for pipe calibration is shown in Fig. 21. The device can realize the calibration process of large thin-walled pipes.

As shown in Fig. 21, the roller is connected with the slider fixed on the frame via bearing. The slider can slide vertically along the frame surface via a screw to adjust the radial reduction of the three rollers. The support assembly keeps the balance of the pipe during the experiment. The servo motor drives two lower rollers to rotate synchronously,

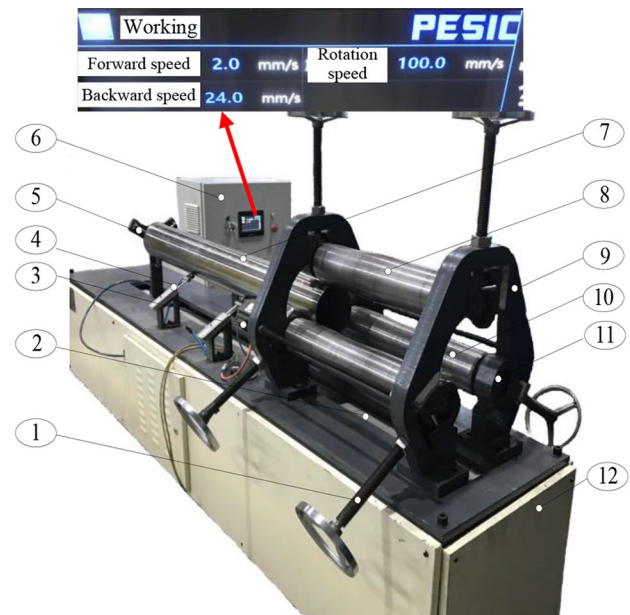**Fig. 20** Change of the upper rollers' loading force with time

Fig. 21 Experimental device for pipe calibration. 1, screw; 2, lead screw drive; 3, servo motor; 4, support assembly; 5, push plate; 6, control cabinet; 7, pipe; 8, upper roller; 9, frame; 10, lower roller; 11, slider; 12, pedestal

Table 5 Experimental results after calibration

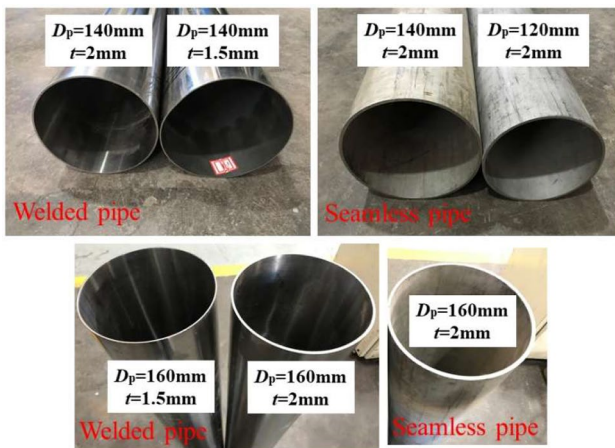| Material	Length L_p (mm)	Initial ovality	Initial straightness		Outer diameter D_p (mm)	Thickness t (mm)	Residual ovality (%)	Residual Straightness (‰)
304	1000	5%	10‰	Welded pipe	140	2	0.61	1.7
						1.5	0.65	1.8
					160	2	0.58	1.6
						1.5	0.62	1.7
				Seamless pipe	140	2	0.60	1.6
					120		0.72	1.7
					160		0.71	1.6

Fig. 22 Forming effect of 304 pipes

which drives the pipe and the upper roller to start turning. At the same time, the push plate drives the pipe to move along the slideway. So far, the calibration process of simultaneous rotation and movement of the pipe is realized. The pipes and rollers selected for the experiment are the same as the pipes and rollers selected for the simulation.

The experimental results of 304 pipes after calibration are shown in Table 5. From Table 5, it can be observed that the residual ovality is within 0.7% and the residual straightness is within 0.2%. Both meet industry standard requirements [1]. The experimental results further verify that the calibration process of pipes is achieved. The forming effect of 304 pipes is shown in Fig. 22.

6 Conclusions

1. Based on previous research, the three-roller continuous and synchronous calibration process of straightness and ovality for large thin-walled pipes is feasible. To explore the influence of the weld on this process, a comparative study of welded pipes and seamless pipes is done using FE method.

2. The FEM of this process is established according to the experimental results of the micro-tensile experiment and the Vickers hardness test of the actual welded pipe. According to micro-tensile test, it is thought that the materials of the parent and the weld zone of 304 pipe are isotropic, respectively. In addition, the mechanical properties parameters are further obtained. With Vickers hardness test, the size of the weld zone is determined, with analyzing its microstructure performance.

3. The FE results show that there is a slight distortion at the inlet end of the welded pipe, and its length is 20 mm. The maximum deviation value is 0.55 mm. Distortion regions and deviation values are small and are found to be negligible. The difference between welded pipes and seamless pipes about the residual straightness and residual ovality is very small. The residual straightness does not exceed 2‰, and the residual ovality is not more than 1%. The changed trend of each roller with time of the welded pipe is almost consistent with the change trend of seamless pipe.

4. Experimental results and FE results demonstrate good agreement. This calibration process of straightness and ovality has been demonstrated to be effective for both welded pipes and seamless pipes.

Author contribution Xueying Huang: conceptualization, methodology, validation, formal analysis, investigation, data curation, writing—original draft, writing—review and editing, software, visualization. Jun Zhao: conceptualization, methodology, formal analysis, supervision, writing—review and editing. Gaochao Yu: conceptualization, methodology, formal analysis, supervision. Rongzhi Li: conceptualization, methodology, formal analysis, supervision. Bangbang Ma: conceptualization, methodology, formal analysis, supervision. Chunge Wang: conceptualization, methodology, formal analysis, supervision.

Declarations

Ethics approval The authors declare that this manuscript was not submitted to more than one journal for simultaneous consideration. Also,

the submitted work is original and has not been published elsewhere in any form or language.

Consent to participate and consent for publication The authors declare that they participated in this paper willingly and the authors declare to consent to the publication of this paper.

Conflict of interest The authors declare no competing interests.

References

1. ANSI/API Specification 5L, Specification for line pipe (forty-fifth edition). Washington DC, United States, 2012.
2. Deng D, Murakawa H, Liang W (2008) Numerical and experimental investigations on welding residual stress in multi-pass butt-welded austenitic stainless-steel pipe. Comput Mater Sci 42(2):234–244. https://doi.org/10.1016/j.commatsci.2007.07.009
3. Law M, Prask H, Luzin V, Gnaeupel-Herold T (2006) Residual stress measurements in coil linepipe and girth welded pipe. Mater Sci Eng, A 437(1):60–63. https://doi.org/10.1016/j.msea.2006.04.062
4. Yaghi A, Hyde TH, Becker AA, Sun W, Williams JA (2008) Residual stress simulation in thin and thick-walled stainless steel pipe welds including pipe diameter effects. Int J Press Vessels Pip 83(11–12):864–874. https://doi.org/10.1016/j.ijpvp.2006.08.014
5. Yin J, Zhao J, Qu XY, Zhai RX (2011) Springback analysis of expanding and setting round for large diameter pipe. J Mechanical Eng 47(12):32–42. https://doi.org/10.3901/JME.2011.12.032
6. Yin J, Zhao J, Sun HL, Zhan PP (2011) Precise compression and setting round by mould for large pipes. Opt Precis Eng 19(9):2072–2078. https://doi.org/10.3788/OPE.20111909.2072
7. Zhao J, Zhan PP, Ma R, Zhai RX (2012) Control strategy of over-bending setting round for pipe-end of large pipes by mould press type method. Transactions of Nonferrous Metals Society of China 22(S2):329–334. https://doi.org/10.1016/S1003-6326(12)61727-0
8. Zhao J, Zhan PP, Ma R, Zhai RX (2013) Quantitative prediction of reduction in large pipe setting round process. Chinese Journal of Mechanical Engineering (English Edition) 26(4):722–729
9. Zhao J, Zhan PP, Ma R, Zhai RX (2014) Prediction and control of springback in setting round process for pipe-end of large pipe. Int J Press Vessels Pip 116(1):56–64. https://doi.org/10.1016/j.ijpvp.2014.01.006
10. Zhao J, Yu GC, Ma R (2016) A mechanical model of symmetrical three-roller setting round process: the static bending stage. J Mater Process Technol 231:501–512. https://doi.org/10.1016/j.jmatprotec.2016.01.002
11. Yu GC, Zhao J, Xing JJ, Zhao FP, Li SL (2017) Research on the symmetrical three-roller setting round process. Journal of Mechanical Engineering 53(14):136–143. https://doi.org/10.3901/JME.2017.14.136
12. Zhao J, Song XK, Cao HQ, Liu J (2014) Press straightening control strategy of multi-step three-point bending for LSAW pipes. J Harbin Institute of Technol 46(1):90–96. https://doi.org/10.11918/j.issn.0367-6234.2014.01.016
13. Zhao J, Song XK, Cao HQ, Liu J (2014) Principle of multi-point bending one-off straightening process for longitudinally submerged arc welding pipes. Journal of Mechanical Engineering 50(2):92–97. https://doi.org/10.3901/JME.2014.02.092
14. Liu ZJ, Ma LD, Li JH, Du YK, Meng ZJ (2020) Accuracy analysis of six skewed-roll straightening process of tube. J Iron and Steel Res 32(9):55–61. https://doi.org/10.13228/j.boyuan.issn1001-0963.20200014
15. Wang CG, Yu GC, Wang W, Zhao J (2018) Deflection detection and curve fitting in three-roll continuous straightening process for LSAW pipes. J Mater Process Technol 255:150–160. https://doi.org/10.1016/j.jmatprotec.2017.11.060
16. Wang CG, Zhang ZY, Zhai RX, Yu GC, Zhao J (2018) Cross-sectional distortion of LSAW pipes in over-bend straightening process. Thin-Walled Structures 129(AUG.): 85–93. https://doi.org/10.1016/j.tws.2018.03.016
17. Cui F, Yang HL (2015) New understanding in the field of straightening theory. Heavy Machinery. https://doi.org/10.3969/j.issn.1001-196X.2015.01.001
18. Huang XY, Yu GC, Zhai RX, Ma R, Zhou C, Gao CL, Zhao J (2021) Roller design and numerical simulation of three-roller continuous and synchronous adjusting straightness and roundness process on LSAW pipes. J Mechanical Eng 57(10):148–159. https://doi.org/10.3901/JME.2021.10.148
19. Zhao J, Yu GC, WANG HR (2017) A roller-type continuous and synchronous calibrating straightness and roundness equipment and processing method for pipes. Hebei: CN106623507A, 2017–05–10
20. Huang XY, Yu GC, Sun HL, Zhao J (2021) A mechanical model of axial and circumferential bidirectional deformation for large thin-walled pipes in the process of continuous and synchronous calibration of roundness and straightness by three rollers. Int J Adv Manuf Technol 116(11/12):3809–3826. https://doi.org/10.1007/s00170-021-07479-4
21. Herynk MD, Kyriakides S, Onoufriou A, Yun HD (2007) Effects of the UOE/UOC pipe manufacturing processes on pipe collapse pressure. Int J Mechanical Sci 49(5):533–553. https://doi.org/10.1016/j.ijmecsci.2006.10.001
22. Chatzopoulou G, Karamanos SA, Varelis GE (2014) Effects of UOE manufacturing process on pressurized bending response of offshore pipes. In ASME Proceedings of the 2014 10th International Pipeline Conference V003T07A039. https://doi.org/10.1115/IPC2014-33321
23. Kyriakides S, Herynk MD, Yun H (2006) Optimization of UOE pipe manufacturing process for improved collapse performance under external pressure. In ASME Proceedings of the 2006 International Pipeline Conference, 355362. https://doi.org/10.1115/IPC2006-10614
24. Chatzopoulou G, Karamanos SA, Varelis GE (2016) Finite element analysis of UOE manufacturing process and its effect on mechanical behavior of offshore pipes. Int J Solids Struct 83:13–27. https://doi.org/10.1016/j.ijsolstr.2015.12.020
25. Pourahmadi M, Saybani M (2022) Reliability analysis with corrosion defects in submarine pipeline case study: oil pipeline in Abkhark island. Ocean Eng 249:110885. https://doi.org/10.1016/J.OCEANENG.2022.110885
26. Dong ZQ, Zhang JX (2018) Three-dimensional finite element analysis of residual stresses in circumferential welds of 2205/X65 bimetallic pipe. Int J Adv Manuf Technol 96(5/8):2841–2851. https://doi.org/10.1007/s00170-018-1698-2
27. Velázquez JC, González-Arévalo NE, Díaz-Cruz M, Cervantes-Tobón A, Herrera-Hernández H, Hernández-Sánchez E (2022) Failure pressure estimation for an aged and corroded oil and gas pipeline: a finite element study. J Natural Gas Sci Eng 101
28. Wu G, Luo JH, Xu GD, Zhu LX, Li LF, Chen CC (2019) Effect of prestrain on strain response characteristics and tensile properties of X80 line pipe steel with weld zones. Nat Gas Ind 39(7):120–126. https://doi.org/10.3787/j.issn.1000-0976.2019.07.016
29. Vishnu M, Hariharan K, Shrabani M (2020) Analysis of UOE forming process accounting for Bauschinger effect and welding. Mater Manuf Processes 35(5/8):910–921. https://doi.org/10.1080/10426914.2020.1745230

30. Huang XY, Zhao J, Yu GC, Meng QD, Mu ZK, Zhai RX (2021) Three-roller continuous setting round process for longitudinally submerged arc welding pipes. Transactions of Nonferrous Metals Society of China 31(5):1411–1426. https://doi.org/10.1016/S1003-6326(21)65586-3

31. Liu HL, Liu YL, Du XY (2020) Cross-sectional deformation of high strength steel rectangular welded tube in rotary draw bending with different constitutive relationships. Int J Adv Manuf Technol 107(9–10):4333–4344. https://doi.org/10.1007/s00170-020-05293-y

32. Huang XY, Yu GC, Wang CG, Zhao J (2022) Deformation mechanism analysis of three-roller continuous and synchronous calibration process of straightness and roundness for LSAW pipes. Int J Adv Manuf Technol 121:1731–1742. https://doi.org/10.1007/s00170-022-09426-3